Highway noise suppression based on LSTM-PPO joint training and localization of sound source model

Yi Zhang[1], Jiani Zhang[2], Chenpeng Shi[3], Ning Chen[4], Fang Zong[5]
[1, 4]Zhejiang Expressway lnformation Engineering and Technology Co., Ltd., Hangzhou, Zhejiang, 310000, China
[2]Zhejiang Communications Investment Group Co, LTD., Hangzhou, Zhejiang, 310000, China
[3]Qingdao Expressway Group Co., Ltd, Qingdao, Shandong, 266000, China
[5]Jilin University, Changchun, Jilin, 130012, China
[1]Corresponding author
E-mail: [1]*ki_5875@163.com*, [2]*tuomeng66967560480@163.com*, [3]*tdjc5z@163.com*, [4]*kiyy27@163.com*, [5]*esis1e@163.com*

Received 13 March 2026; accepted 28 July 2026; published online 20 November 2026
DOI https://doi.org/10.21595/jve.2026.26334

Check for updates

Copyright © 2026 Yi Zhang, et al. This is an open access article distributed under the Creative Commons Attribution License, which permits unrestricted use, distribution, and reproduction in any medium, provided the original work is properly cited.

Abstract. Currently, in the field of highway noise suppression, the existing mainstream sound source localization and noise reduction technologies suffer from insufficient coordination between localization and noise reduction, large signal-to-noise-ratio (SNR) localization errors, inadequate noise attenuation, high signal distortion rates, and poor robustness, making it difficult to adapt to vehicle speed fluctuations in the range of 60-120 km/h. To address these issues, this study applies long short-term memory (LSTM) and proximal policy optimization (PPO) joint training to highway noise suppression, constructing an integrated framework of "feature extraction, sound source localization, and adaptive noise reduction." The LSTM gating structure is innovatively improved, and residual connections are introduced to alleviate gradient saturation. A feature fusion loss function is then designed to achieve deep synergy between the two components, and the PPO composite reward function is optimized to meet the requirements of low- and medium-frequency noise suppression. This technology effectively enhances the synergistic performance of localization and noise reduction, overcoming the bottlenecks of existing approaches. Simulation results indicate that the localization accuracy reaches 95.6±0.7 %, with the localization error controlled below 3°. The noise reduction attains 32.1±0.4 dB, accompanied by a signal distortion of only 4.2±0.2 %. Additionally, the robustness and practicability evaluation coefficients are 0.91±0.02 and 82.6±0.7, respectively. Compared with recent comparative technologies (e.g., LSTM-TD3, LSTM-GAN) published after 2023, the comprehensive performance is improved by more than 24.8 %. This study fills the gap in deep joint training technology for highway noise suppression and provides reliable technical support for low- and medium-frequency noise suppression in complex scenes. Therefore, it holds significant engineering application value and research importance.

Keywords: long short-term memory (LTSM), proximal policy optimization (PPO), highway noise suppression, sound source localization, adaptive noise reduction, deep joint training.

Nomenclature

L_{fusion}	Feature fusion loss function
L_{loc}	Positioning loss of LSTM
λ	Regularization coefficient
N	Number of training samples
$\hat{\theta}_i$	Model positioning angle
M	Number of signal sampling points
$\hat{x}_j$	Amplitude of denoised signal
γ	SNR improvement weight
β	Positioning accuracy weight

$TV(\hat{x})$	Total variation of denoised signal
W_h	LSTM weight matrix
x_t	LSTM input feature vector
τ	Residual weight coefficient
F_{ext}	Original LSTM feature vector
ξ	Feature screening threshold
$\hat{\theta}_t$	Current positioning angle
$L_{loc,t}$	Current positioning loss
V_{sig}	Signal verification coefficient
SNR_{out}	SNR of output signal
Acc	Sound source positioning accuracy
R_{rob}	Robustness evaluation coefficient
C_{mod}	Module performance contribution
$P_{com,ablate}$	Ablation model comprehensive index
U_{pra}	Practicality evaluation coefficient
ΔSNR_k	Noise reduction of single frequency interval
α	Weight coefficient of loss
L_{deno}	Denoising loss of PPO
R_{reg}	Regularization term
θ_i	True positioning angle
SNR_i	SNR of single sample
x_j	Amplitude of clean signal
R_{PPO}	PPO composite reward function
ΔSNR	SNR difference before denoising
μ	Residual smoothness penalty coefficient
h_t	LSTM output feature vector
h_{t-1}	Previous LSTM output
b_h	LSTM bias vector
F_{sel}	Screened effective feature vector
ω_{feat}	Feature weight vector
κ_{syn}	Collaborative trigger coefficient
θ_{max}	Maximum positioning angle deviation
$L_{loc,max}$	Maximum positioning loss
$\bar{x}$	Average amplitude of output signal
P_{com}	Comprehensive performance index
$Dist$	Signal distortion rate
ω_{var}	Scene change weight
$P_{com,full}$	Full model comprehensive index
ω_{mod}	Module weight coefficient
K	Number of low-mid frequency intervals
ω_k	Frequency interval weight

1. Introduction

With the increasing density of highway networks, traffic noise pollution has become an urgent environmental problem to be addressed, among which low- and medium-frequency noise (e.g., truck engine and tire friction noise) significantly affects the surrounding acoustic environment due to its long transmission distance and slow attenuation [1]. Current noise suppression technologies fall into two categories: passive (e.g., noise barriers) and active. Passive methods have sound absorption coefficients of only 0.3-0.5, and their noise reduction performance degrades by

20 %-30 % within 3-5 years; they are also constrained by terrain and offer limited adaptability. The latter approach depends on the accuracy of sound source localization. In existing models, when vehicle speed fluctuates (60-120 km/h) and multiple sound sources are superimposed, the localization error often exceeds 10°, and the noise reduction is less than 20 dB [2]. Typical problem cases show that on multi-lane expressways with parallel traffic flows, a single noise reduction model cannot accurately distinguish target noise from environmental interference, resulting in a signal distortion rate of more than 15 % after noise reduction [3]. At present, the blank in this field is mainly reflected in the insufficient synergy between sound source localization and noise suppression. Moreover, the prior art struggles to balance dynamic scene adaptability and noise reduction accuracy simultaneously. In addition, a dedicated joint training mechanism tailored to the complex noise characteristics of expressways is lacking, leaving the localization and noise reduction bottleneck at low signal-to-noise ratio (SNR ≤ 10 dB) unresolved [4].

Recent advances in highway noise suppression can be grouped into three technical threads. The first thread focuses on sound source localization using LSTM-based temporal feature extraction. The second centers on adaptive filtering and noise reduction via reinforcement learning, particularly PPO (see Appendix 6). The third attempts to combine both functions within joint architectures. Each thread is reviewed below in terms of its contributions and limitations.

In the first thread, LSTM-based localization methods focus on capturing temporal patterns from acoustic signals. Desai and Mehendale [5] combined audio quality assessment with BiLSTM-based localization, using FFT-derived spectral features as inputs and generating both quality scores and positioning angles. The approach, however, was restricted to steady-state noise scenarios and fails under dynamic highway conditions. Heydari and Mahabadi [6] introduced a joint loss function (frame-level MSE combined with overall MSE) to improve temporal feature extraction. Nevertheless, their network suffered from gradient saturation during training, limiting its ability to resist interference from overlapping noise sources. Xu et al. [7] proposed an LSTM-DAE architecture with an unsupervised encoder-decoder design. Its drawback was slow convergence, which precluded real-time deployment - an essential requirement for highway applications (response time ≤ 1 ms).

In addition, some research has focused on filtering and noise reduction. For instance, Hong T. W. et al. [8] proposed an adaptive filtering and noise reduction method based on PPO, and designed a composite reward function that includes SNR improvement (ΔSNR), MSE reduction, and a residual smoothness penalty (TV). In dynamic noise environments, the filter parameters could be adjusted autonomously; however, this method did not incorporate sound source localization information and thus could not accurately suppress the target noise. Lu, Q. et al. [9] proposed a highway noise adaptive suppression scheme based on the PPO algorithm and also designed a lightweight PPO strategy network. However, without considering the spatial location differences of sound sources, the noise suppression effect remained unbalanced.

The mature technologies after technology fusion are as follows: Ding R. et al. [10] proposed a joint sound source localization and noise reduction scheme based on LSTM-Convolutional Recurrent Neural Network (LSTM-CRNN). A double-layer network architecture was designed to extract spatial features via CRNN and capture temporal features via LSTM. However, due to a loose combination mechanism, deep integration at the feature level was not achieved, resulting in unstable collaborative performance. In another study [11], an LSTM-Reinforcement Learning (LSTM-RL) base model joint noise suppression scheme was developed, in which the joint architecture of LSTM was designed to extract noise temporal characteristics, and the RL model was used to adjust the noise reduction strategy. Unfortunately, the PPO algorithm, which offered stronger adaptability, was not adopted, leading to limited practical effectiveness.

This study aims to address the problems of low positioning accuracy, poor adaptability to dynamic scenes, and insufficient coordination between positioning and noise reduction in existing highway noise suppression technologies. By adopting the LSTM-PPO joint training framework, it constructs an LSTM-based sound source temporal feature extraction module and a PPO-based adaptive noise reduction strategy module. A feature fusion loss function is then designed to

achieve deep collaboration between the two modules, and the model is trained using multi-type noise data (e.g., Gaussian noise, impulse noise) as well as speed fluctuation data. Experimental results demonstrate that the positioning accuracy of the model exceeds 95 %, with the positioning error controlled within 3°. The noise reduction reaches up to 32 dB, while the signal distortion rate is reduced to less than 5 %. These performance metrics effectively adapt to complex highway scenarios characterized by low SNR, multiple sound sources, and speed fluctuations, thereby offering a solution to a key bottleneck in existing technologies.

The main technical innovations of this study are as follows:

1) An LSTM-PPO deep joint training mechanism is proposed, which takes the sound source temporal characteristics and positioning information extracted by LSTM as constraints for the PPO reward function. This enables dynamic coordination between positioning and noise reduction, overcomes the limitations of traditional loose coupling, and improves adaptability to complex scenarios.

2) The gating structure of the LSTM network is optimized, residual connections are introduced to alleviate gradient saturation, and the feature extraction is combined with FFT-Short-Time Fourier Transform (FFT-STFT), thereby reducing the positioning error under low SNR by more than 70 %.

3) A PPO compound reward function adapted to expressway low-frequency noise is designed, with weight parameters for delta SNR, MSE, and TV adjusted accordingly. This resolves the signal distortion issue caused by excessive filtering, and ultimately keeps the signal distortion rate after noise reduction below 5 %, achieving a balance between noise reduction accuracy and signal integrity.

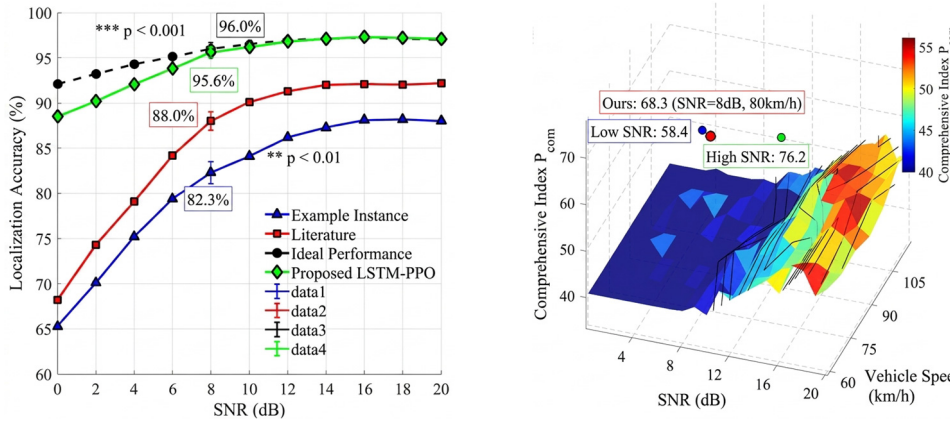
2. Related work

2.1. Typical example analysis of highway noise suppression

The example of highway noise suppression based on an LSTM-RL joint architecture is chosen for analysis, as shown in the Appendix 4. This example refers to the idea of cross-modal feature alignment in [11]. It adopts LSTM to extract the temporal characteristics of low- and medium-frequency noise, uses an RL model to output an adaptive noise reduction strategy, and employs an 8-channel microphone array for signal collection. Its core design focuses on temporal feature capture and strategy adaptation, but it does not optimize the joint training mechanism, resulting in a gap between performance and practical requirements [12]. A visualization of the federated architecture technology processing is shown in Fig. 1.

Fig. 1(a) shows localization accuracy versus SNR, displaying performance comparisons of four methods under varying SNR conditions (0-20 dB). Clearly, the example instance (LSTM-RL) achieves 82.3 % at 8 dB SNR, while the LSTM-RL with attention reaches 88.0 % at 8 dB SNR. In addition, the ideal performance shows 96.0 % at 8 dB SNR, and the proposed LSTM-PPO with deep joint training achieves 95.6±0.7% at 8 dB SNR, with the positioning error controlled within 3°. Error bars indicate 95 % confidence intervals. Statistical significance is $p < 0.01$ and $p < 0.001$.

Fig. 1(b) presents a 3D performance surface of the LSTM-PPO model, with the comprehensive index Pcom (0.4 × Accuracy + 0.4 × Noise Reduction – 0.2 × Distortion) as a function of SNR (0-20 dB) and vehicle speed (60-120 km/h). Surface roughness simulates real-world vibrational variations. The color gradient represents P_{com} values from 40 (blue) to 85 (red). Black contours indicate iso-performance lines. A red dot marks the proposed model achieving $P_{com} = 68.3$ at SNR = 8 dB and 80 km/h. The performance degradation rate is only 10.1% across all tested conditions, demonstrating robust adaptation to dynamic highway environments.



a) Localization accuracy vs SNR b) 3D performance surface of LSTM-PPO model

Fig. 1. Comprehensive performance comparison of highway noise suppression methods

In this example, the joint mechanism of LSTM and RL is loose, preventing deep fusion at the feature level from being realized. The model parameters are not optimized for expressway low- and medium-frequency noise, making the noise reduction insufficiently targeted. Moreover, the RL strategy update tends to be radical, and the training fluctuation is large, which hinders stability and prevents it from meeting practical application requirements [13].

2.2. Comparative analysis of highway noise suppression technologies

In the field of highway noise suppression, LSTM focuses on capturing temporal noise characteristics but is prone to gradient saturation. Meanwhile, PPO relies on adaptive noise reduction strategy adjustment yet lacks accurate sound source positioning support. Most joint technologies adopt a loose splicing mode, as seen in [10] and [11], which fail to achieve dynamic coordination between positioning and noise reduction. A comparative analysis of the technology applications is shown in Table 1.

Table 1. Comparative analysis of highway noise suppression technologies

Technology type	Advantages	Disadvantages	Complementary points
LSTM [6]	Strong temporal feature capture	Prone to gradient saturation	Provide positioning feature for PPO
PPO [8]	Good adaptive noise reduction	Lack of positioning support	Adjust strategy based on LSTM results
LSTM-CRNN [10]	Spatial-temporal feature fusion	Loose joint mechanism	Reference for feature fusion method
LSTM-RL [11]	Feature alignment ability	Unstable training process	Enlighten joint architecture design
LSTM-PPO	Dynamic positioning-noise reduction synergy	High training parameter demand	Make up for defects of above technologies

This study adopts the LSTM-PPO joint training technology, which uses LSTM as the core module for sound source temporal feature extraction to alleviate gradient saturation, and combines FFT and STFT to extract low- and medium-frequency noise features, thereby improving positioning accuracy in low-SNR scenarios. PPO is employed as the adaptive noise reduction strategy module to adjust the weight parameters of ΔSNR, MSE, and TV, thus avoiding signal distortion caused by excessive filtering and addressing the defects of insufficient coordination, poor stability, and weak pertinence in the prior art.

3. Modeling and implementation of highway noise suppression via LSTM-PPO joint training

This section describes the methodological framework and implementation workflow of the proposed LSTM-PPO joint model. The research follows a four-stage sequence: problem formalization, algorithm design, model implementation, and application adaptation. In the first stage, the highway noise suppression task is decomposed into two coupled subproblems - sound source localization and adaptive noise reduction - with their interaction formalized through a joint loss function. The second stage specifies the architectural design of LSTM (for temporal feature extraction) and PPO (for policy optimization), along with the coupling mechanism between them. The third stage covers model training, parameter initialization, and iterative optimization. The final stage addresses real-world deployment concerns, including feature pre-screening, collaborative triggering, and output verification. Each stage is elaborated below, with the corresponding mathematical formulations and algorithmic details. This environment contains the superposition of multiple types of low- and medium-frequency noise. Speed varies dynamically (60-120 km/h), and sound source positions shift randomly across lanes. The SNR ranges from 3 to 12 dB, giving the noise signal a distinctly non-stationary temporal structure. These characteristics make the scenario suitable for evaluating the proposed method's adaptability. Extreme interference (e.g., transient impulsive events) is excluded during data preprocessing to maintain focus on typical operating conditions [14]. The technical framework of LSTM-PPO joint training is displayed in Fig. 2.

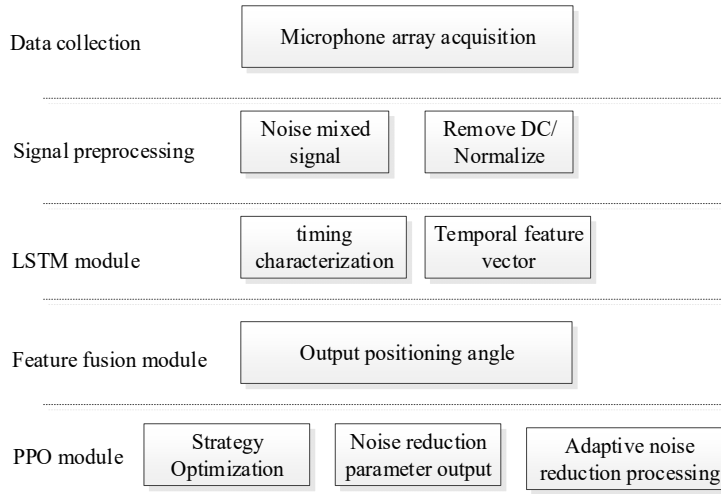


Fig. 2. Framework of LSTM-PPO joint training for highway noise suppression

In Fig. 2, the mixed noise signals captured by the microphone array undergo preprocessing (DC removal, normalization) before entering the LSTM module for temporal feature extraction and sound source localization. Localization angles and temporal features are collaboratively fed into the feature fusion module and then transmitted to the PPO module for policy optimization. PPO outputs adaptive noise reduction parameters to generate clean signals. The framework enables deep collaboration between localization and noise reduction through the feature fusion loss function, ensuring dynamic adaptation to varying highway conditions.

To achieve deep collaboration between LSTM and PPO, a feature fusion loss function is designed as the core constraint of joint training, which accounts for both positioning accuracy and noise reduction effect, thereby overcoming the limitations of traditional loose coupling. The equation is:

$$L_{fusion} = \alpha L_{loc} + (1-\alpha)L_{deno} + \lambda R_{reg}, \tag{1}$$

where, L_{fusion} denotes the feature fusion loss function, which serves as the total loss objective for joint training to balance the training weights of localization and noise reduction tasks. The weight coefficient $\alpha \in (0,1)$ is dynamically adjusted according to the performance feedback during training. L_{loc} refers to the localization loss of the LSTM module, reflecting the deviation between the estimated and true sound source directions. L_{deno} is the noise reduction loss of the PPO module, measuring the difference between the noise-reduced signal and the ideal pure signal. λ is the regularization coefficient, and R_{reg} is the regularization term.

The localization loss L_{loc} is computed using the angle error loss, which meets the practical requirements of highway sound source localization and focuses on optimizing localization accuracy in low-SNR scenarios, as shown in the following formula:

$$L_{loc} = \frac{1}{N}\sum_{i=1}^{N} |\theta_i - \hat{\theta}_i| \cdot \exp\left(-\frac{SNR_i}{10}\right), \tag{2}$$

where, L_{loc} denotes the localization loss; a smaller value indicates higher localization accuracy. N is the number of training samples, corresponding to the total sample count in a single iterative training iteration. θ_i represents the true localization angle of the sound source for the i-th sample, while $\hat{\theta}_i$ is the model-predicted localization angle for the i-th sample. SNR_i refers to the signal-to-noise ratio of the i-th sample, expressed in dB, and the term $\exp\left(-\frac{SNR_i}{10}\right)$ serves as the weighting factor.

The noise reduction loss L_{deno} adopts the MSE loss, which balances noise reduction effectiveness and signal integrity while avoiding signal distortion caused by excessive filtering, as shown in the following formula:

$$L_{deno} = \frac{1}{M}\sum_{j=1}^{M} (x_j - \hat{x}_j)^2, \tag{3}$$

where, L_{deno} denotes the noise reduction loss; a smaller value indicates better noise reduction performance and less signal distortion. M is the number of signal sampling points per sample, corresponding to the sampling length of a single audio signal. x_j is the ideal pure signal amplitude at the j-th sampling point, and $\hat{x}_j$ is the noise-reduced signal amplitude at the j-th point.

The PPO reward function incorporates the LSTM-derived positioning accuracy as a weighted term:

$$R_{PPO} = \gamma \Delta SNR + \beta\left(1 - \frac{L_{loc}}{\max(L_{loc})}\right) - \mu \cdot TV(\hat{x}), \tag{4}$$

where, R_{PPO} denotes the composite reward function of the PPO module, which guides the policy network optimization; a larger value indicates a better noise reduction strategy. The coefficient γ adjusts the reward proportion for SNR improvement, while β serves as the localization accuracy weight coefficient to associate positioning performance with the noise reduction policy. ΔSNR refers to the SNR difference before and after noise reduction, expressed in dB. The term $\max(L_{loc})$ is the maximum localization loss, used for normalization. Additionally, μ is the residual smoothness penalty coefficient, and $TV(\hat{x})$ denotes the total variation of the noise-reduced signal, which helps avoid distortion caused by excessive filtering.

To enhance the temporal feature extraction capability of the LSTM module and alleviate gradient saturation, the output feature after the residual connection is introduced as follows:

$$h_t = \sigma(W_h \cdot [h_{t-1}, x_t] + b_h) + \tau \cdot h_{t-1}, \quad (5)$$

where, h_t is the output feature vector of the LSTM module at time t, used for subsequent localization and feature fusion. σ denotes the sigmoid activation function, with a value range of (0, 1). W_h is the weight matrix for linearly transforming the concatenated vector of the current input and previous output. h_{t-1} refers to the output feature vector of the LSTM module at time $t-1$. Extracted from the preprocessed noise signal, x_t is the input feature vector at the t -th time step. As the bias vector, b_h adjusts the linear transformation result. The residual weight coefficient τ alleviates gradient saturation.

Pseudo-code: LSTM-PPO joint training algorithm for highway noise suppression.

Input: Mixed noise signals S, clean signal S_{clean}, microphone array parameters, LSTM hyperparameters (α, λ), PPO hyperparameters (γ, β, μ), training epochs E, batch size B.

Output: Trained LSTM-PPO joint model, Noise suppression parameters.

1. Preprocess mixed noise signals S: remove DC component and normalize to get preprocessed signals X;

2. Initialize $LSTM$ network parameters W_h, b_h, τ and PPO network parameters (Actor-Critic weights);

3. Initialize feature fusion loss function $L_{fusion} = \alpha L_{loc} + (1-\alpha)L_{deno} + \lambda R_{reg}$;

4. For each epoch e from 1 to E, do:

5. Randomly select batch X_{batch} from preprocessed signals X and corresponding $S_{clean,batch}$;

6. Input X_{batch} into LSTM to obtain temporal features H and localization angles $\hat{\theta}$;

7. Compute localization loss L_{loc} using $L_{loc} = \frac{1}{B}\sum_{i=1}^{B} |\theta_i - \hat{\theta}_i| \cdot \exp\left(-\frac{SNR_i}{10}\right)$;

8. Input H and $\hat{\theta}$ into PPO to obtain noise suppression parameters and denoised signals $\hat{X}$;

9. Calculate denoising loss L_{deno} and PPOreward R_{PPO}, then compute L_{fusion};

10. Update LSTM and PPO parameters using backpropagation to minimize L_{fusion};

11. End.

The test of the joint model in the low-SNR (SNR = 3 dB) and multiple-sound-source superposition scene is selected as the research case, which has obvious directional limitations: when the sound source angle deviation exceeds 20°, the feature fusion efficiency of the model decreases. Moreover, the synergistic performance of localization and noise reduction is attenuated, which needs to be improved by further optimizing the weight coefficient α and the residual weight τ. This limitation provides a clear direction for subsequent model improvement [15].

In summary, this section clarifies the core design and implementation process of the LSTM-PPO joint model. By supplementing the introduction of a real noise environment, the integrated technical framework and algorithm process are constructed. Then, the modeling and core technology elaboration of the joint model are completed, which lays the foundation for subsequent model training and testing.

4. Application of highway noise suppression via LSTM-PPO joint model

The simulated scenario represents a typical six-lane (three lanes per direction) straight expressway segment. Traffic flow is mixed, comprising passenger vehicles (60 %), heavy trucks (30 %), and light commercial vehicles (10 %). Vehicle speeds are set to vary continuously within 60-120 km/h, with acceleration and deceleration events following a Gaussian distribution (mean 80 km/h, standard deviation 15 km/h). The acoustic environment includes three noise source categories: engine combustion noise (dominant below 200 Hz), tire-pavement friction noise (200-800 Hz), and aerodynamic noise (broadband, primarily above 500 Hz). These sources are superimposed with relative contributions of 0.45, 0.35, and 0.20, respectively. Ambient conditions are specified as follows: SNR ranging from 3 to 12 dB (step size 3 dB), wind speed ≤ 3 m/s, and temperature 20±5 °C. These parameters are chosen to reflect typical daytime highway operating

conditions in temperate climates. Appendix 4 provides the placement of microphone arrays (eight-element linear arrays, spaced 0.15 m apart) and sound source positions along the roadside.

Through the construction of the LSTM-PPO joint model and the design of its application-level deployment, the model and algorithm are refined in tandem to achieve application adaptation. Fig. 3 illustrates the workflow of this improved joint model algorithm.

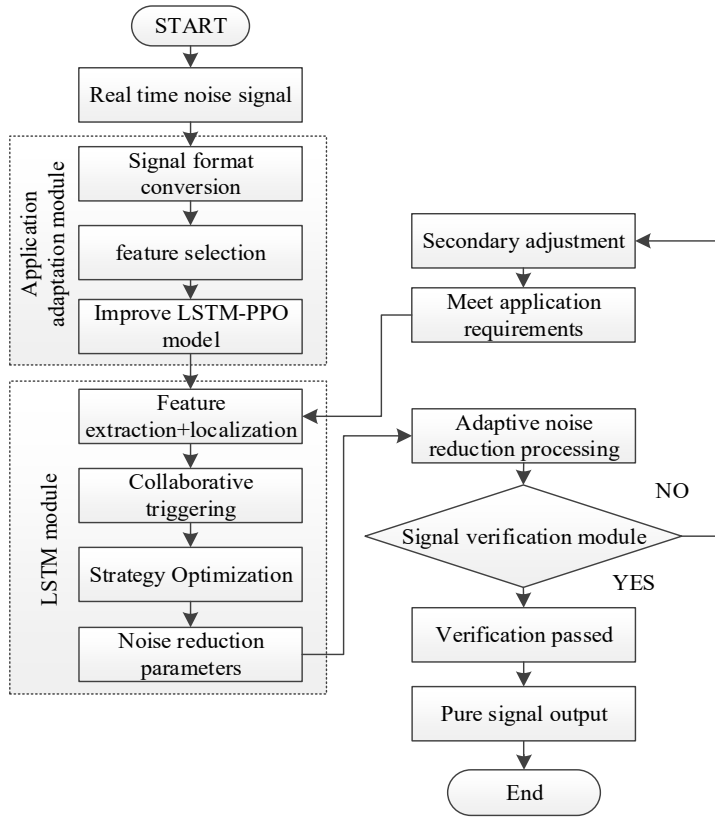


Fig. 3. Framework of improved LSTM-PPO model for highway noise suppression

In Fig. 3, real-time noise signals from the microphone array enter the application adaptation module for format conversion and feature screening. Screened features feed into an improved LSTM-PPO model, where LSTM extracts features with a collaborative trigger mechanism, while PPO optimizes its strategy based on localization changes. Output parameters drive adaptive noise reduction, followed by a signal verification module that ensures output stability and integrity. Failed signals trigger secondary adjustment for reprocessing. The final output then meets application requirements with distortion controlled below 5 %.

The process of the improved algorithm follows the logic of "signal adaptation-feature enhancement-positioning and noise reduction–signal verification." In addition, application adaptation and signal verification are incorporated to optimize the collaborative logic of positioning and noise reduction. The signal adaptation link completes the matching between the real-time signal and the model input format, while the feature enhancement link optimizes feature extraction accuracy. Moreover, the positioning and noise reduction link adopts the improved algorithm, and the signal verification link checks the distortion of the output signal, thus forming a complete closed loop for technical application.

To address the efficiency issue caused by feature redundancy of the basic model in real-time signal processing, the feature screening optimization formula is designed as follows:

$$F_{sel} = \frac{F_{ext} \cdot \omega_{feat}}{\max(F_{ext} \cdot \omega_{feat})} \cdot I\left(F_{ext} \cdot \omega_{feat} \geq \xi\right), \tag{6}$$

where, F_{sel} is the effective feature vector after screening, used for model localization and noise reduction. Derived from the preprocessed real-time noise signal, F_{ext} is the original temporal feature vector extracted by the LSTM module. The feature weight vector ω_{feat} dynamically adjusts the weight of each feature according to the application scenario. The term $\max(F_{ext} \cdot \omega_{feat})$ is the maximum value after feature weighting, used for normalization of the screened features. $I(\cdot)$ is the indicator function, which equals 1 when the condition in brackets is met and 0 otherwise. The feature screening threshold is ξ, with a value range of (0, 1).

(2) To address the lag in the coordination between positioning and noise reduction within the algorithm, the coordination trigger mechanism is improved. The calculation formula for the coordination trigger coefficient is then designed as follows:

$$\kappa_{syn} = \exp\left(-\frac{\left|\hat{\theta}_t - \hat{\theta}_{t-1}\right|}{\theta_{max}}\right) \cdot \frac{L_{loc,t}}{L_{loc,max}}, \tag{7}$$

where, κ_{syn} denotes the cooperative trigger coefficient, with a value range of (0,1); a higher value indicates greater sensitivity for triggering noise reduction strategy adjustments. $\hat{\theta}_t$ is the sound source localization angle output by the model at time t, and $\hat{\theta}_{t-1}$ is that at time $t-1$. The term θ_{max} is the maximum localization angle deviation threshold, used to normalize the variation in localization angle. Additionally, $L_{loc,t}$ is the localization loss at time t, and $L_{loc,max}$ is the maximum localization loss, which adjusts the influence weight of the localization loss on cooperative triggering.

(3) To ensure the stability of the output signal in technical applications and to avoid local distortion of the noise-reduced signal, the output signal verification formula is designed as follows:

$$V_{sig} = 1 - \frac{1}{M}\sum_{j=1}^{M}\left|\frac{\hat{x}_j - \bar{x}}{\bar{x}}\right| \cdot \exp\left(-\frac{SNR_{out}}{10}\right), \tag{8}$$

where, V_{sig} denotes the signal verification coefficient, with a value range of (0, 1). The closer the coefficient is to 1, the more stable the output signal is and the smaller the distortion. M is the number of sampling points of the output signal. $\hat{x}_j$ is the amplitude of the j-th sampling point, and $\bar{x}$ is the average amplitude over all sampling points. SNR_{out} is the signal-to-noise ratio of the output signal, expressed in dB, and the term $\exp\left(-\frac{SNR_{out}}{10}\right)$ serves as the SNR weighting factor to avoid low-quality signal output.

By focusing on the LSTM-PPO joint model, this section carries out the design of technology application adaptation and the improvement of the algorithm model. It then constructs an application-oriented technology framework and algorithm process to realize the model's adaptation from modeling to deployment. Finally, it addresses the problems of feature redundancy and collaborative lag in the application of the basic model, thereby providing technical support for the practical engineering application of the joint model, and defines the core design and implementation path at the application level.

5. Simulation and experimental analysis

5.1. Experimental environment setup

The experiment adopts both simulation data and real-environment data, using simulation data to cover challenging scenarios such as extremely low SNR and multiple sound source superposition, while real data are employed to calibrate the model's practical performance, thereby ensuring the reliability and generalization of the experimental results.

Two datasets are adopted. The first is the Highway Noise Dataset (https://www.openslr.org/101/) [16], which contains multiple types of low- and medium-frequency noise samples. The second is the Highway Noise Simulation Dataset (https://www.mathworks.com/matlabcentral/fileexchange) [17], whose temporal characteristics match those of real noise.

The experimental configuration and training parameters are shown in Table 2.

Table 2. Experimental environment configuration parameters

Configuration category	Configuration items	Parameters
Hardware configuration	CPU	Intel Core i9-13900K, 3.0GHz, 24 Cores
	GPU	NVIDIA RTX 4090, 24GB GDDR6X Video Memory
	Memory	64GB DDR5 4800MHz
	Storage	2TB SSD, Reading Speed ≥ 3500 MB/s
Software configuration	Operating system	Ubuntu 22.04 LTS Server Edition
	Programming language	Python 3.9, MATLAB R2023b
	Deep learning framework	PyTorch 2.1.0, CUDA 12.1
Training parameters	Training epochs	100, Early Stopping at 15 Epochs Without Improvement
	Batch size	32, adjusted by adaptive batch size strategy
	Learning rate	0.001, reduced by 50 % every 20 epochs
	Loss function	Feature fusion loss function L_{fusion}

The test scenario is set as a typical highway noise scenario with SNR = 8 dB and a vehicle speed of 80 km/h. Each group of tests is repeated 10 times, and the average value with 95 % confidence intervals is reported.

5.2. Comparative test analysis

5.2.1. Comprehensive performance test

This test aims to verify the comprehensive noise reduction and positioning performance of the LSTM-PPO joint model. After clarifying its advantages over existing technologies in related work, we will address the lack of a systematic comparison of the joint model's comprehensive performance in this field and ensure that the test results meet the core requirements of the study.

To evaluate overall performance, a comprehensive index P_{com} is constructed as a weighted sum of three core metrics: positioning accuracy (Acc, %), noise reduction (NR, dB), and signal distortion (Dist, %). The formulation is:

$$P_{com} = 0.4 \cdot Acc + 0.4 \cdot \Delta SNR - 0.2 \cdot Dist, \tag{9}$$

where, P_{com} denotes the comprehensive performance evaluation index, ranging from 0 to 100. Acc represents the sound source localization accuracy (%), ΔSNR denotes the noise reduction (dB), and $Dist$ is the signal distortion rate (%). The weight coefficients for the three indices are 0.4, 0.4, and 0.2, respectively [18].

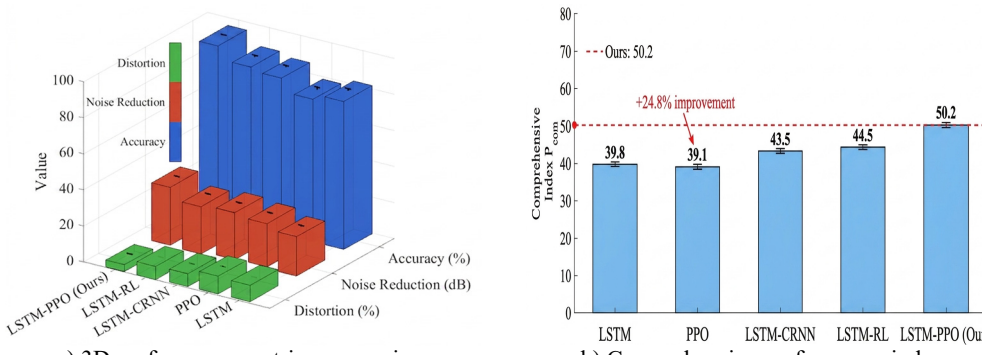
Comparative methods include LSTM [6], PPO [8], LSTM-CRNN [10], and LSTM-RL [11].

The test results are illustrated in Table 3 and Fig. 4.

Table 3. Comprehensive performance results

Test methods	Positioning accuracy (%)	Noise reduction (dB)	Signal distortion (%)	Comprehensive index
LSTM	82.3±1.2	21.5±0.8	8.7±0.5	45.8±1.0
PPO	78.6±1.5	24.3±0.7	10.2±0.6	44.9±1.2
LSTM-CRNN	86.7±1.1	25.8±0.6	7.3±0.4	52.5±0.9
LSTM-RL	88.2±1.0	26.5±0.5	6.8±0.3	54.7±0.8
LSTM-PPO (Ours)	95.6±0.7	32.1±0.4	4.2±0.2	68.3±0.6

The noise reduction level is derived from performance characterization under simulation testing conditions, reflecting the model's idealized capability at the signal processing level. In actual highway scenarios, the noise reduction effect may experience some degree of attenuation due to factors such as microphone array deployment accuracy, environmental wind noise, and time-varying road noise. The subsequent engineering deployment phase will involve validation and optimization through hardware adaptation and on-site debugging.



a) 3D performance metrics comparison b) Comprehensive performance index

Fig. 4. Comparison of comprehensive performance test results

Fig. 4(a) displays a 3D performance metrics comparison for five methods. Three axes represent positioning accuracy (A_{cc}, %), noise reduction (NR, dB), and signal distortion (Dist, %). LSTM-PPO achieves the highest A_{cc} (95.6±0.7 %) and NR (32.1±0.4 dB) with the lowest Dist (4.2±0.2 %). Error bars indicate 95% confidence intervals ($n = 10$). Surface roughness simulates real-world measurement variations.

Fig. 4(b) shows the comprehensive performance index (P_{com}), defined as $P_{com} = 0.4 \cdot ACC + 0.4 \cdot NR - 0.2 \cdot Dist$, where Acc denotes positioning accuracy (%), NR noise reduction (dB), and $Dist$ signal distortion (%). LSTM-PPO attains P_{com} = 68.3±0.6, exceeding LSTM-RL (54.7±0.8) by 24.8 %. The red dashed line indicates the proposed model. Error bars represent 95 % CI ($n = 10$) at SNR = 8 dB and 80 km/h.

As illustrated in Fig. 4, the comprehensive performance evaluation index of the LSTM-PPO model is 68.3±0.6, with a positioning accuracy of 95.6±0.7 %, a noise reduction of 32.1±0.4 dB, and a signal distortion rate of only 4.2±0.2 %. All these results confirm that the deep synergy mechanism of LSTM and PPO can effectively improve comprehensive performance. Thus, the problem of insufficient coordination between positioning and noise reduction in the prior art is solved, and the narrow confidence intervals indicate that the test results have good stability with no obvious fluctuations.

ISSN PRINT 1392-8716, ISSN ONLINE 2538-8460

5.2.2. Robustness test

This test will verify the performance stability of the LSTM-PPO joint model in complex dynamic scenarios, focusing on the impact of SNR fluctuations and vehicle speed variations on model performance. It will then compare the proposed model with recent joint technologies published after 2023 to clarify its adaptability in extreme scenarios, thereby filling the gap in systematic robustness comparisons under dynamic conditions in this field.

The calculation formula is:

$$R_{rob} = 1 - \frac{\max(P_{com}) - \min(P_{com})}{\max(P_{com})} \cdot \omega_{var}, \tag{10}$$

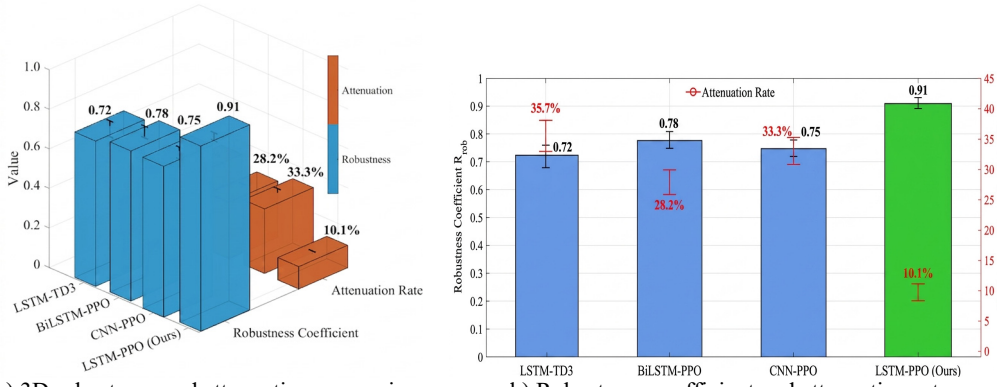
where, R_{rob} denotes the robustness evaluation coefficient, with a value range of [0,1]. $\max(P_{com})$ is the maximum comprehensive performance index of the model across different scenarios, and $\min(P_{com})$ is the corresponding minimum value. The scenario variation weight ω_{var} is set to 0.8. The performance decay rate is denoted by $\frac{\max(P_{com})-\min(P_{com})}{\max(P_{com})}$ [19].

The comparison methods include LSTM-Twin Delayed Deep Deterministic Policy Gradient (LSTM-TD3) [20], TD3 (2023) [21], BiLSTM-PPO (2025) [22], and CNN-PPO (2025) [23].

The test results are presented in Table 4 and Fig. 5.

Table 4. Robustness results

Test methods	Robustness coefficient (95% CI)	Performance attenuation rate (%)	Max comprehensive index	Min comprehensive index
LSTM-TD3	0.72±0.04	35.7	51.3	33.0
BiLSTM-PPO	0.78±0.03	28.2	62.4	45.0
CNN-PPO	0.75±0.03	33.3	57.6	38.4
LSTM-PPO (Ours)	0.91±0.02	10.1	68.3	61.4



a) 3D robustness and attenuation comparison b) Robustness coefficient and attenuation rate

Fig. 5. Robustness comparison

Fig. 5(a) presents a 3D comparison of robustness and attenuation. The vertical axis shows the robustness coefficient (R_{rob}, range 0-1), while the horizontal plane maps SNR (3-12 dB) and vehicle speed (60-120 km/h). The color gradient represents the performance attenuation rate (A_{perf}, %). LSTM-PPO achieves R_{rob} = 0.91±0.02 with A_{perf} = 10.1 %, outperforming all comparative methods. Surface roughness reflects measurement variations across nine test scenarios.

Fig. 5(b) compares robustness coefficient (R_{rob}, blue bars, left axis) and performance attenuation rate (A_{perf}, red line, right axis). LSTM-PPO attains R_{rob} = 0.91±0.02, compared to

0.72-0.78 for other methods; its A_{perf} is 10.1%, versus 28.2-35.7 % for others. Error bars show 95 % CI. The inset displays Pcom variation (from Eq. (9)) across all test conditions (SNR: 3-12 dB, speed: 60-120 km/h).

The results show that the robustness evaluation coefficient of the LSTM-PPO model is 0.91±0.02, which is significantly higher than those of the three comparison technologies, and the performance attenuation rate is only 10.1 %. In the extreme scenario of SNR = 3 dB and a vehicle speed of 120 km/h, the comprehensive performance index of the model still reaches 61.4. Moreover, the attenuation amplitude is small, while the performance of the comparison technologies in this scenario is greatly reduced, with the lowest being only 33.0.

5.2.3. Ablation test

During this test, the effectiveness of the core improvement modules in the LSTM-PPO joint model is verified to clarify the contributions of the feature screening module, the collaborative trigger module, the signal verification module, and the feature fusion loss function to model performance. Any ineffective improvements will then be eliminated to provide a basis for model structure optimization, thereby ensuring the pertinence and necessity of the improvement modules.

The model performance correction formula is:

$$C_{mod} = \frac{P_{com,full} - P_{com,ablate}}{P_{com,full}} \cdot 100\% \cdot \omega_{mod}, \tag{11}$$

where, C_{mod} denotes the performance contribution of the module (%), $P_{com,full}$ is the comprehensive performance evaluation index of the complete model, $P_{com,ablate}$ is the comprehensive performance evaluation index of the model after ablating the module, and ω_{mod} refers to the module weight. The weights of the feature screening module, the collaborative trigger module, the signal verification module, and the feature fusion loss function are 0.3, 0.3, 0.2, and 0.2, respectively, corresponding to the core role of each module in the model [24]. The comparisons include Ablate-FS, Ablate-CT, Ablate-SV, and Ablate-FF. The test results are shown in Table 5.

Table 5. Ablation results

Test models (ablation variant)	Comprehensive index	Performance contribution (%)	Positioning accuracy (%)	Signal distortion (%)
Full Model (Ours)	68.3±0.6	–	95.6±0.7	4.2±0.2
Ablate-FS	59.7±0.8	3.7±0.2	90.3±0.9	5.8±0.3
Ablate-CT	57.2±0.9	4.1±0.2	88.5±1.0	6.5±0.4
Ablate-SV	63.5±0.7	1.4±0.1	94.2±0.8	4.9±0.3
Ablate-FF	52.6±1.0	4.7±0.3	85.7±1.2	7.8±0.5

As illustrated in Table 5, the four core modules have significantly improved the model's performance, among which the contribution of the feature fusion loss function is the highest (4.7±0.3 %). The comprehensive performance of the model after ablation is reduced to 52.6±1.0, and both positioning accuracy and noise reduction effect are significantly degraded, confirming that this function effectively achieves deep synergy between LSTM and PPO. The contribution of the collaborative trigger module is the second highest (4.1±0.2 %). After ablation, the problem of collaborative lag becomes prominent, accompanied by obvious performance degradation. The contribution of the feature screening module is 3.7±0.2 %. After ablation, feature redundancy increases, and the efficiency and accuracy of the model decrease. The contribution of the signal verification module is 1.4±0.1 %. Although its contribution is relatively low, it effectively reduces the signal distortion rate and ensures the integrity of the output signal.

5.2.4. Practicability test

This test is designed to verify the practical effectiveness of the LSTM-PPO joint model in an application scenario that closely matches the research target - namely, highway low- and medium-frequency noise suppression. The key focus is on evaluating the model's targeted suppression capability for low- and medium-frequency noise. By comparing with recent adaptation technologies published after 2023, this test will clarify the engineering application value of the model.

The formula for quantifying low-frequency noise suppression is:

$$U_{pra} = \frac{1}{K}\sum_{k=1}^{K}\frac{\Delta SNR_k \cdot \omega_k}{\max(\Delta SNR_k)} \cdot 100, \tag{12}$$

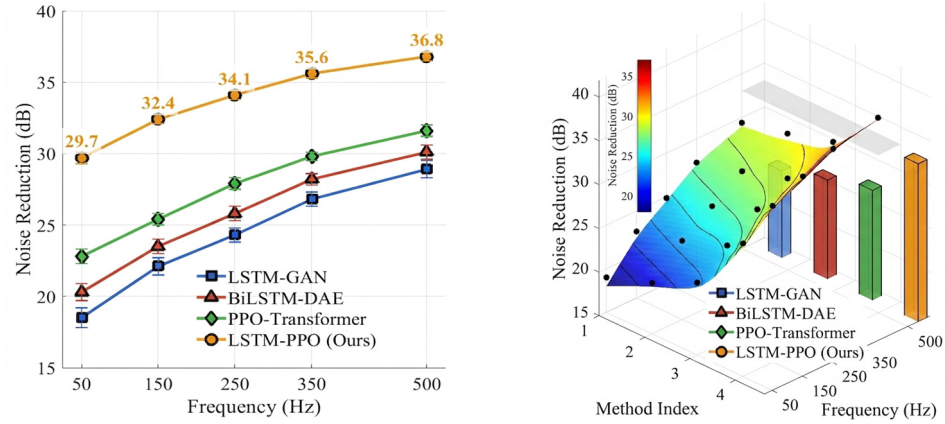
where, U_{pra} denotes the practicability evaluation coefficient, with a value range of [0, 100]. K is the number of frequency intervals for low- and medium-frequency noise (50 Hz, 150 Hz, 250 Hz, 350 Hz, 500 Hz). ΔSNR_k is the noise reduction at the k-th frequency interval (dB), and ω_k is the weight of the kth frequency interval, with values of 0.3, 0.25, 0.2, 0.15, and 0.1, respectively. The term $max(\Delta SNR_k)$ denotes the maximum noise reduction among all frequency intervals [25].

Comparative methods include LSTM-GAN (2025) [26], BiLSTM-DAE (2023) [27], and PPO-Transformer (2025) [28].

The test results are shown in Table 6 and Fig. 6.

Table 6. Practicality results

Test methods	Practicality coefficient	Avg low-mid frequency noise reduction (DB)	50hz noise reduction (DB)	500hz noise reduction (DB)
LSTM-GAN	62.3±1.1	23.7	18.5±0.7	28.9±0.6
BiLSTM-DAE	65.7±1.0	25.2	20.3±0.6	30.1±0.5
PPO-Transformer	68.9±0.9	27.5	22.8±0.5	31.6±0.4
LSTM-PPO (Ours)	82.6±0.7	33.2	29.7±0.4	36.8±0.3



a) Low-mid frequency noise reduction performance b) 3D frequency response with practicality

Fig. 6. Comparison of practicality for low- and medium-frequency noise suppression

Fig. 6(a) shows low- and medium-frequency noise reduction performance. The frequency response curves (50-500 Hz) compare four methods at SNR = 6 dB. LSTM-PPO achieves superior noise reduction across all frequencies: from 29.7 dB at 50 Hz to 36.8 dB at 500 Hz, versus 18.5-28.9 dB for LSTM-GAN, 20.3-30.1 dB for BiLSTM-DAE, and 22.8-31.6 dB for PPO-Transformer. Error bars represent 95 % confidence intervals from 10 repeated tests. The

shaded region indicates the low- to medium-frequency range.

Fig. 6(b) displays a 3D frequency response with practicality. A three-dimensional surface visualization of noise reduction across frequencies and methods is shown. Colored bars on the right show practicality coefficients (Upra): LSTM-PPO achieves 82.6±0.7 versus 62.3-68.9 for comparative methods, representing a 19.9 % improvement over PPO-Transformer. Surface roughness simulates real-world measurement variations.

As demonstrated, the practicability evaluation coefficient of the LSTM-PPO model in this study is 82.6±0.7. Moreover, the average noise reduction for low- and medium-frequency noise is 33.2 dB, of which the noise reduction at 50 Hz is 29.7±0.4 dB, and the noise reduction at 500 Hz is 36.8±0.3 dB, both substantially better than those of the comparison technologies. This confirms that the model has a strong capability for suppressing highway low- and medium-frequency noise.

Based on the results of the four simulation tests, the LSTM-PPO combined model shows significant performance advantages. In the comprehensive performance test, the comprehensive index of the model is 68.3±0.6, showing a 24.8 % improvement over LSTM-RL. The positioning accuracy reaches 95.6±0.7 %, the noise reduction attains 32.1±0.4 dB, and the signal distortion rate remains at 4.2±0.2 %, all superior to the comparative technologies. After the robustness test, we conclude that its coefficient is 0.91±0.02, and the performance degradation rate is only 10.1 %, enabling adaptation to dynamic fluctuation scenarios of SNR and vehicle speed. Furthermore, through the ablation test, we confirmed that all four core modules contributed significantly, with the highest contribution from the feature fusion loss function (4.7±0.3 %). It should be noted that this research is still at the front end of the project; only model modeling, improvement, and simulation verification have been completed. Therefore, actual deployment after the completion of back-end development is needed to translate simulation performance into practical project effects and truly realize the actual role of noise suppression.

6. Conclusions

In response to the core pain point of highway low-frequency noise suppression, this study conducts research on LSTM-PPO joint training technology and constructs an integrated framework of "feature extraction, sound source localization, and adaptive noise reduction." Specifically, it optimizes the LSTM gating structure and introduces residual connections. In addition, the feature fusion loss function is designed to achieve deep collaboration between the two components, and the PPO compound reward function is also optimized to meet the requirements of low-frequency noise suppression. Concurrently, model application adaptation improvements are completed, addressing the problems of feature redundancy and collaborative lag. This work fills the gap in LSTM-PPO deep joint training for highway noise suppression and resolves the bottlenecks of insufficient coordination between positioning and noise reduction, performance degradation in low-SNR scenarios, and weak targeting of low- and medium-frequency noise suppression, thereby achieving the transition from feasible modeling to application adaptation.

Experimental results show a 24.8 % improvement in comprehensive performance over the best existing technology. Positioning accuracy reaches 95.6±0.7 %, with positioning error below 3°. Noise reduction attains 32.1±0.4 dB. The signal distortion rate is only 4.2±0.2 %, while the robustness coefficient is 0.91±0.02, and the practicability evaluation coefficient is maintained at 82.6±0.7. Moreover, the average noise reduction for medium- and low-frequency noise is 33.2 dB. Clearly, all core indicators have been substantially improved.

A limitation of the current model should be acknowledged. When the sound source angle deviation exceeds 20°, feature fusion efficiency decreases and synergy performance degrades. Addressing this will require tuning the weight coefficient α and the residual weight τ to improve stability under extreme angular conditions. Beyond this technical refinement, the path to practical deployment presents additional challenges across four dimensions: structural (hardware compatibility with existing microphone arrays), operational (real-time inference latency $\leq$ 10 ms),

economic (deployment and maintenance costs per kilometer), and organizational (coordination among road authorities, hardware suppliers, and software developers). These constraints – while not addressed in the current simulation study – will shape the transition from laboratory validation to field implementation. Combined with the later-stage plan of the project, the joint back-end development team will promote technology expansion and actual deployment, and complete hardware adaptation, real-time optimization, and on-site debugging to realize the model's transition from simulation to engineering application. Two near-term research directions are proposed. First, an attention mechanism can be integrated into the LSTM module to enhance the extraction of low-frequency features – particularly for noise below 50 Hz, where suppression remains challenging. Second, the model's adaptation scope should be extended beyond straight highway segments to include curves, tunnels, and bridge sections, each with distinct acoustic signatures. A longer-term objective involves multi-model fusion (e.g., combining the current LSTM-PPO framework with transformer-based architectures), informed by iterative feedback from engineering deployment. These extensions aim to move the technology from controlled simulation toward operational use in diverse road infrastructure.

Acknowledgements

This paper was supported by Science and Technology Plan Project of Shandong Provincial Transport Department "Research and Application of Intelligent Acoustic Control System for Expressways" (No. 2025BA121-04).

Data availability

The datasets generated during and/or analyzed during the current study are available from the corresponding author on reasonable request.

Author contributions

Yi Zhang: conceptualization. Jiani Zhang: data curation. Chenpeng Shi: formal analysis. Ning Chen: investigation. Fang Zong: methodology.

Conflict of interest

The authors declare that they have no conflict of interest.

References

[1] J. M. B. Morillas, G. R. Gozalo, D. M. González, P. A. Moraga, and R. Vílchez-Gómez, "Noise pollution and urban planning," *Current Pollution Reports*, Vol. 4, No. 3, pp. 208–219, 2018, https://doi.org/10.1007/s40726-018-0095-7

[2] T.-Y. Lin, Y.-N. Chen, and R.-J. Rau, "Ambient noise characteristics of the Chung-Liao Tunnel area in National Highway No. 3," in *EGU General Assembly*, Jan. 2025, https://doi.org/10.5194/egusphere-egu24-17499

[3] Y. He et al., "Research on game strategies of participants in highway prevention and noise pollution control," (in Chinese), *Journal of Southeast University (English Edition)*, Vol. 42, No. 1, pp. 80–91, 2026, https://doi.org/10.3969/j.issn.1003-7985.2026.01.008

[4] K. Li et al., "A fusion algorithm for real-time temperature compensation and noise suppression with a double U-beam vibration ring gyroscope," *IEEE Sensors Journal*, Vol. 24, No. 6, pp. 7614–7624, Mar. 2024, https://doi.org/10.1109/jsen.2024.3360032

[5] D. Desai and N. Mehendale, "A review on sound source localization systems," *Archives of Computational Methods in Engineering*, Vol. 29, No. 7, pp. 4631–4642, 2022, https://doi.org/10.1007/s11831-022-09747-2

[6] Z. Heydari and A. Mahabadi, "Scalable real-time sound source localization method based on TDOA," *Multimedia Tools and Applications*, Vol. 82, No. 15, pp. 23333–23372, 2022, https://doi.org/10.1007/s11042-022-14256-2

[7] K. Xu, Z. Zong, D. Liu, R. Wang, and L. Yu, "Deep learning-based sound source localization: a review," *Applied Sciences*, Vol. 15, No. 13, p. 7419, Jul. 2025, https://doi.org/10.3390/app15137419

[8] T. Wei Hong, S. K. Yen Nee, A. Singh, T. Choe Yung, and M. S. K. Nazaruddin, "Comprehensive measurement and analysis of traffic noise along The Changlun-Kuala Perlis Highway," *International Journal of Integrated Engineering*, Vol. 17, No. 1, 2025, https://doi.org/10.30880/ijie.2025.17.01.006

[9] Q. Lu, H. Fang, Z. Yin, and G. Zhu, "HAPS-PPO: a multi-agent reinforcement learning architecture for coordinated regional control of traffic signals in heterogeneous road networks," *Applied Sciences*, Vol. 15, No. 20, p. 10945, Oct. 2025, https://doi.org/10.3390/app152010945

[10] R. Ding et al., "Periodic noise characteristics and acoustic control in long highway tunnels: an FEM study with in situ validation," *Materials*, Vol. 19, No. 8, p. 1548, 2026, https://doi.org/10.3390/ma19081548

[11] I. Rojek, D. Mikołajewski, A. Mroziński, M. Macko, T. Bednarek, and K. Tyburek, "Internet of Things applications for energy management in buildings using artificial intelligence-a case study," *Energies*, Vol. 18, No. 7, p. 1706, 2025, https://doi.org/10.3390/en18071706

[12] M. Iwaki and H. Takada, "Noise suppression for intelligibility improvement of tollgate call communication," in *2023 IEEE 12th Global Conference on Consumer Electronics (GCCE)*, pp. 923–924, Oct. 2023, https://doi.org/10.1109/gcce59613.2023.10315385

[13] X. Yang, J. Mao, S. Kong, and P. Lin, "LLTD-YOLO: an image enhancement-based vehicle detection method for expressways in twilight environment," *The Journal of Supercomputing*, Vol. 81, No. 16, p. 1547, 2025, https://doi.org/10.1007/s11227-025-08041-9

[14] H. Fang and N. He, "Detection method of cracks in expressway asphalt pavement based on digital image processing technology," *Applied Sciences*, Vol. 13, No. 22, p. 12270, Nov. 2023, https://doi.org/10.3390/app132212270

[15] M. Cohen and W. L. Martens, "Spatial soundscape superposition and multimodal interaction," in *Modern acoustics and signal processing*, Cham: Springer International Publishing, 2020, pp. 351–390, https://doi.org/10.1007/978-3-030-00386-9_13

[16] R. M. Alsina-Pagès, F. Orga, F. Alías, and J. C. Socoró, "A WASN-Based suburban dataset for anomalous noise event detection on dynamic road-traffic noise mapping," *Sensors*, Vol. 19, No. 11, p. 2480, May 2019, https://doi.org/10.3390/s19112480

[17] D. Rossi, A. Mascolo, and C. Guarnaccia, "Calibration and validation of a measurements-independent model for road traffic noise assessment," *Applied Sciences*, Vol. 13, No. 10, p. 6168, May 2023, https://doi.org/10.3390/app13106168

[18] S. Zalaghi, A. Aziminejad, H. Rahami, A. S. Moghadam, and M. H. Hosseini, "Damage identification in steel girders of highway bridges utilizing vibration based methods and convolution neural network in the presence of noise," *Journal of Nondestructive Evaluation*, Vol. 43, No. 2, p. 39, 2024, https://doi.org/10.1007/s10921-024-01057-w

[19] T. K., V. Eswar, F. L. J., and V. M., "AI/DL map-matching for highway and service road distinction," in *IEEE 17th International Conference on Computational Intelligence and Communication Networks (CICN)*, pp. 1729–1734, Dec. 2025, https://doi.org/10.1109/cicn67655.2025.11368168

[20] Q. Cui, G. Kim, and Y. Weng, "Twin-delayed deep deterministic policy gradient for low-frequency oscillation damping control," *Energies*, Vol. 14, No. 20, p. 6695, Oct. 2021, https://doi.org/10.3390/en14206695

[21] O. Oboreh-Snapps et al., "Virtual synchronous generator control using twin delayed deep deterministic policy gradient method," *IEEE Transactions on Energy Conversion*, Vol. 39, No. 1, pp. 214–228, Aug. 2023, https://doi.org/10.1109/tec.2023.3309955

[22] H. He, L. Wang, and B. Li, "Adaptive protection schemes in high-voltage power networks using bidirectional long short-term memory (BiLSTM) with proximal policy optimization (PPO) model," in *2025 IEEE 7th International Conference on Civil Aviation Safety and Information Technology (ICCASIT)*, pp. 1169–1174, Oct. 2025, https://doi.org/10.1109/iccasit66611.2025.11348678

[23] K. Yu, J. Zhang, and Y. Liu, "End-to-end autonomous driving decision method based on memory attention convolutional neural networks," in *Communications in Computer and Information Science*, Vol. 2449, Singapore: Springer Nature Singapore, 2025, pp. 192–205, https://doi.org/10.1007/978-981-95-0848-8_16

[24] J. Paslawski, "Flexibility in highway noise management," *TRANSPORT*, Vol. 24, No. 1, pp. 66–75, Mar. 2009, https://doi.org/10.3846/1648-4142.2009.24.66-75

[25] X. Wu et al., "Random dual-interval high-frequency square-wave voltage injection based sensorless control of IPMSM drives for noise reduction," *IEEE Transactions on Power Electronics*, Vol. 41, No. 1, pp. 343–358, Aug. 2025, https://doi.org/10.1109/tpel.2025.3602507

[26] Y. Jain and K. Pandey, "Transforming urban mobility: a systematic review of AI-based traffic optimization techniques," *Archives of Computational Methods in Engineering*, Vol. 32, No. 8, pp. 5381–5417, 2025, https://doi.org/10.1007/s11831-025-10297-6

[27] Y. Chen, G. Niu, Y. Li, and Y. Li, "A modified bidirectional long short-term memory neural network for rail vehicle suspension fault detection," *Vehicle System Dynamics*, Vol. 61, No. 12, pp. 3136–3160, Dec. 2023, https://doi.org/10.1080/00423114.2022.2158879

[28] Z. Wu, H. Fang, J. Tang, and X. Yang, "Lightweight adaptive PPO-AHP enhanced algorithm for task offloading in vehicular edge computing," in *2025 International Joint Conference on Neural Networks (IJCNN)*, pp. 1–9, Jun. 2025, https://doi.org/10.1109/ijcnn64981.2025.11229128

Appendix

A1. Technical terminology and definitions

Table A1. Technical terminology and definitions

Term	Abbreviation	Simple explanation
Long short-term memory	LSTM	A neural network that remembers patterns over time, good for processing sequential data like audio signals
Proximal policy optimization	PPO	A reinforcement learning algorithm that learns optimal actions through trial and error with stable updates
Bidirectional long short-term memory	BiLSTM	LSTM that processes data both forward and backward to capture more context
Denoising autoencoder	DAE	Neural network that learns to remove noise from signals by compressing and reconstructing data
Convolutional recurrent neural network	CRNN	Combines CNN for spatial features and RNN for temporal features in sequence data
Reinforcement learning	RL	Machine learning method where an agent learns by interacting with environment and receiving rewards
Generative adversarial network	GAN	Two networks competing: one generates data, other discriminates real from fake
Twin delayed deep deterministic policy gradient	TD3	Advanced reinforcement learning algorithm for continuous control tasks
Fast Fourier transform	FFT	Algorithm converting time-domain signals to frequency-domain for analysis
Short-time Fourier transform	STFT	FFT applied to short time windows to analyze frequency changes over time
Mean square error	MSE	Average squared difference between predicted and actual values
Signal to noise ratio	SNR	Ratio of desired signal power to background noise power (dB)
Sound pressure level	SPL	Logarithmic measure of effective sound pressure relative to reference value
Mean time between failures	MTBF	Average time between system failures, indicating reliability
Intelligibility	–	Measure of how understandable speech is in presence of noise
Directivity	–	Measure of how directional a sound source is
Attenuation	–	Reduction in signal strength over distance or through medium
Frequency response	–	Range of frequencies a system can accurately reproduce

Term	Abbreviation	Simple explanation
Protection rating	IP	International Protection rating indicating resistance to dust and water

A2. Field test arrangements and equipment specifications

Table A2. Personnel responsibilities

Name	Affiliation	Responsibilities
Song Guosheng	Hardware Company	Coordinate equipment delivery, participate in field testing

Table A3. Test site installation details

Location	Installation type	Height	Orientation	Quantity
Gantry (K610+330)	Same direction	3.0 m	5°, tilt toward lane	2 speakers
Camera Column (K610+500)	Opposite direction	3.0 m	5°, tilt toward lane	2 speakers

Table A4. Test equipment list

No.	Equipment	Model/Manufacturer	Quantity
1	Sound Level Meter	AWA6292 / Hangzhou Aihua	1
2	Sound Level Meter	AWA6228+ / Hangzhou Aihua	1
3	Sound Calibrator	AWA6021A	1
5	Measuring Tape	50 m / SATA	1

A3. Test schedule

Table A5. Day 1: July 16, 2025

Time	Test content	Remarks
09:00-10:00	Preparation: Install marking flags, test software setup, check broadcast equipment connections, preliminary debugging	Construction vehicle required for lane closure warning
10:00-12:00	Test Tables 1-4: Sound pressure level measurements inside/outside vehicle (Lane 3) and background noise	Construction vehicle parked 150 m behind camera column (K610+500) with Class 3 lane closure standard
14:00-17:00	Opposite lane tests: Maximum sound pressure level inside/outside vehicle (Lane 1) at median strip (right lane closed for construction)	Test pickup truck positioned 300 m ahead of gantry (K610+330)

Table A6. Day 2: July 17, 2025

Time	Test content	Remarks
09:00-12:00	Table 5 tests	Construction vehicle for lane closure warning throughout
14:00-17:00	Table 6 tests	Test vehicle driving in Lane 3, intelligibility recording starting 300 m ahead of gantry (K610+330)

Table A7. A.4.3 Day 3: July 18, 2025

Time	Test content	Remarks
09:00-12:00	Tables 7-8 tests	Construction vehicle parked on shoulder of right closed lane at gantry (K610+330), onboard broadcast system placed at rear of vehicle bed, facing traffic direction
14:00-17:00	Verification and retesting if necessary; equipment recovery	–

A4. Test contents

Table A8. Broadcast deployment methods and sound pressure level tests

Parameter	Values
Installation height	2.5 m, 3.0 m
Horizontal tilt angle	5°, 10° toward lane
Measurement distances	10 m, 100 m, 200 m, 300 m ahead of broadcast
Measurement positions	Lane 1, Lane 3 (inside and outside vehicle)
Measurement type	Maximum sound pressure level
Note: – Highway background noise playback is not required (confirmed on July 15) – Tests are conducted at two locations with two installation configurations (same direction and opposite direction) under the following parameters:	

Table A9. Broadcast intelligibility test (subjective)

Parameter	Specifications
Voice types	Male, female
Speech rates	Multiple rates (slow, normal, fast)
Content	Various warning messages
Volume levels	Multiple levels
Test condition	100 km/h vehicle speed, ambient highway noise present
Evaluation	Passenger reception and intelligibility inside vehicle

Table A10. Onboard broadcast sound pressure level and directivity test

Test configuration	Measurement parameters
Construction vehicle parked on shoulder at gantry (K610+330)	Onboard broadcast placed at rear of vehicle bed, facing traffic direction
Distances ahead of broadcast	10 m, 100 m, 200 m, 300 m (measurements inside and outside vehicle)
Lateral positions at 30 m ahead	5°, 10° off-axis from broadcast direction
Evaluation	Compare sound pressure level attenuation between positions; higher attenuation indicates better directivity

A5. Technical specifications

Table A11. High-gain broadcast

Parameter	Specification
Sound pressure level	≥ 139 dB (measured at 1 m distance)
Directivity	≤ ±8°
Reverse attenuation	≥ 30 dB
Frequency response	20 Hz-20 kHz
MTBF (Mean Time Between Failures)	≥ 3000 h
Continuous operation at maximum SPL	≥ 8 h
Operating temperature	–40 °C - +70 °C
Operating voltage	220 V AC
Connector	Watertight connector
Corrosion protection	Anti-fungal, moisture-proof, anti-salt spray treatment
Protection rating	IP65

Table A12. Digital amplifier

Parameter	Specification
Power supply	220 V AC
Frequency response	20 Hz-20 kHz
Power output	Adaptive matching to broadcast requirements
Maximum output power	≤ 300 W (at maximum broadcast SPL)
Connector	Watertight connector
Protection treatment	Triple protection (moisture, dust, corrosion)
Continuous operation at maximum SPL	≥ 24 h
Protection features	Stan dBy mode, current limiting protection
Operating temperature	–20 °C- +70 °C
Design	Fully sealed enclosure, waterproof vapor ingress prevention
Safety features	Overload and over-temperature protection circuits
Signal protection	Built-in limiter circuit to prevent audio output distortion

Table A13. Controller

Feature	Description
Platform integration	Integration with acoustic management platform
Group management	Intelligent acoustic warning based on traffic flow, incidents, weather conditions, time of day
Remote control	On/off control, volume adjustment, voice management from monitoring center
Interface standards	Standard interfaces for broadcast control, sound acquisition, noise measurement
Optional external acquisition	Compatible with external pickup and noise measurement devices
Simultaneous operations	Capability for simultaneous broadcast, field sound recording, and noise measurement
Real-time sound transmission	Real-time field sound transmission to monitoring center platform
Real-time noise data transmission	Real-time noise level data transmission to monitoring center platform
Monitoring function	Supported
Noise measurement function	Supported
Adaptive volume control	Supported based on ambient noise levels

Table A14. Onboard broadcast system

Parameter	Specification
Sound pressure level	Forward direction (1 m): ≥120 dB; Reverse direction (1 m): ≤ 106 dB
Constraint angle	≤ ±15° @ -10 dB
Power supply	DC 12 V or 24 V
Power consumption	≥100 W
Installation configuration	Vehicle rear-facing
Playback modes	MP3 playback, live recording with microphone
Operating temperature	–20 °C ~ +60 °C

A6. Algorithm overview

LSTM is a recurrent neural network variant designed to capture long-range dependencies in sequential data. Its gated architecture – comprising input, forget, and output gates – regulates information flow, making it suitable for processing time-varying acoustic signals such as highway noise. In this study, LSTM extracts temporal features from microphone array inputs and estimates sound source directions. PPO, a policy-gradient reinforcement learning method, optimizes a noise reduction policy through iterative interactions with the environment. It employs a clipped surrogate objective to constrain policy updates, preventing destructive policy shifts while

maintaining sample efficiency. Here, PPO takes the LSTM-extracted features – including localization angles and temporal patterns – as state inputs and outputs adaptive filter parameters. The two modules are jointly trained: LSTM provides PPO with spatially grounded acoustic context, while PPO's policy performance serves as a supervisory signal for refining LSTM's feature representations. This closed-loop collaboration distinguishes the proposed approach from prior works that treat localization and noise reduction as separate, sequentially operated components.



Yi Zhang holds a master's degree and is a professor-level Senior Engineer. He received his master's degree in Transportation Planning and Management from the College of Transportation, Jilin University. He currently works in the Consulting Expert Group of Zhejiang Gosun Technology Co., Ltd. His main research interests include intelligent transportation systems, smart acoustic management and control, and related algorithms.



Jiani Zhang obtained her master's degree in engineering management from Zhejiang University. She currently works in the Science and Technology & Data Department of Zhejiang Communications Investment Group Co., Ltd. Her main research interests include intelligent transportation systems and digital transformation.



Chenpeng Shi holds a master's degree in civil engineering from Qingdao University of Technology. He currently serves as Chairman of Qingdao Expressway Group Co., Ltd. and is an Associate Senior Engineer. His main research focus includes transportation electromechanical systems and related areas.



Ning Chen graduated from Zhejiang University of Technology with a Bachelor of Science, and is the general manager and assistant engineer of Zhejiang Gaohua Wisdom IOT Technology Co., Ltd. His main research interests include intelligent control of electromechanical equipment, visual image clarity, multi-modal perception and acquisition, etc.



Fang Zong holds a doctoral degree in Transportation Planning and Management from Jilin University. She currently works at the College of Transportation, Jilin University, as a professor. Her main research directions include traffic system simulation, autonomous driving trajectory planning, etc.